Journal of Geodynamics 52 (2011) 432–442

Contents lists available at ScienceDirect

Journal of Geodynamics

journal homepage: http://www.elsevier.com/locate/jog

Lithosphere structures of northeast Tibetan Plateau and their geodynamic implications

Mei Feng[a,*], Meijian An[a], Wenjin Zhao[b], Guangqi Xue[c], James Mechie[d], Yue Zhao[a]

[a] Institute of Geomechanics, Chinese Academy of Geological Sciences, Beijing 100081, China
[b] Chinese Academy of Geological Sciences, Beijing 100037, China
[c] Institute of Mineral Resources, Chinese Academy of Geological Sciences, Beijing 100037, China
[d] Deutsches GeoForschungs Zentrum – GFZ, Section "Geophysical Deep Sounding", Telegrafenberg, 14473 Potsdam, Germany

ARTICLE INFO

Article history:
Received 26 October 2010
Received in revised form 27 June 2011
Accepted 3 July 2011
Available online 14 July 2011

Keywords:
Lithospheric velocity structure
Lithosphere stacking
Bayan Har Terrane
NE Tibetan Plateau

ABSTRACT

In the past ten years, three major earthquakes with devastating impacts have taken place along the margins of the Bayan Har Terrane in NE Tibetan Plateau, China. To understand the geodynamic background controlling the NE Tibetan Plateau, we processed a large amount of broad-band seismic data in and around the Tibetan Plateau, and constructed a three dimensional lithospheric S-wave velocity model using a regional surface-wave tomographic tool. The velocity model produces images of important structures. First, a weak discontinuity at ~110 km depth seems to exist, which separates the abnormally thick Tibetan upper-mantle lithosphere into two layers. Second, the upper-mantle lithospheric velocity structures have certain correlations with seismicity and fault activity. Regions with a low-velocity upper-mantle lithosphere have a stronger seismicity than regions with a high-velocity upper-mantle lithosphere. The earthquake focal mechanisms or faults in the interior of the low-velocity regions typically display normal faulting with a strike-slip component, while reverse faults, sometimes with a small strike-slip component, typically occur in the low-to-high velocity transition zone. The correlation of seismicity and fault activity with upper-mantle lithospheric velocity anomalies suggests that the strength of the upper-mantle lithosphere can control the deformation mode of the overlying crust where most earthquakes occur.

1. Introduction

In the past ten years (2000–2010), the Chinese mainland has been struck by three major earthquakes (indicated as beach balls in Fig. 1) with devastating impacts: the 2001 Mw 7.8 Kunlun earthquake produced a surface rupture zone nearly 400 km in length (Lin et al., 2002), the 2008 Mw 7.9 Wenchuan earthquake killed more than 80,000 people, and the 2010 Mw 6.9 Yushu earthquake killed more than 2000. These earthquakes were all located on the edges of the Bayan Har Terrane (also called the Songpan-Ganze Terrane) in the NE Tibetan Plateau. Thus a study on the lithospheric structures of the Bayan Har Terrane and its surrounding regions is important to understand the geodynamic background controlling the NE Tibetan Plateau, including the seismogenic mechanisms of these earthquakes.

The dark circles in Fig. 1 are earthquakes with a magnitude bigger than 4.0 that have occurred in the study region over the past 40 years (data are from the USGS and Chinese CSN catalogues). As the active period of a seismogenic fault can be hundreds of years, earthquakes that have occurred over a short time such as 40 years cannot be taken as reliable indicators of the intensity of seismicity along different faults. For instance, there are more earthquakes concentrated along the Longmen Shan Fault than on the other faults in Fig. 1, but that does not mean that the Longmen Shan Fault is more active than other faults in a longer term, especially since most of these earthquakes are aftershocks of the 2008 Wenchuan earthquake. However, the seismicity within a tectonic block shows some correlation with the block's fragmentation, density of secondary faults, and relative intensity of tectonic activity. As shown in Fig. 1, most earthquakes of the Bayan Har Terrane have occurred along its boundaries, while the interior of the terrane has experienced fewer earthquakes than the Qiangtang Terrane to the south of it, probably suggesting that the Bayan Har Terrane is, in itself, more stable than the Qiangtang Terrane, but its boundaries are very active.

The Bayan Har Terrane in the NE Tibetan Plateau has a complex evolution history. In the Paleozoic and Mesozoic, its tectonic evolution was mainly controlled by the spreading and subduction of the Tethys Sea plate (Xiao and Li, 2000). It amalgamated with the Eurasian continent (Kunlun-Qaidam Terrane), which was to the north of it, during the late Permian, and then collided and amalga-

* Corresponding author. Tel.: +86 10 13683690618; fax: +86 10 68422326.
E-mail address: mei_feng_cn@yahoo.com.cn (M. Feng).

0264-3707/$ – see front matter © 2011 Elsevier Ltd. All rights reserved.
doi:10.1016/j.jog.2011.07.002

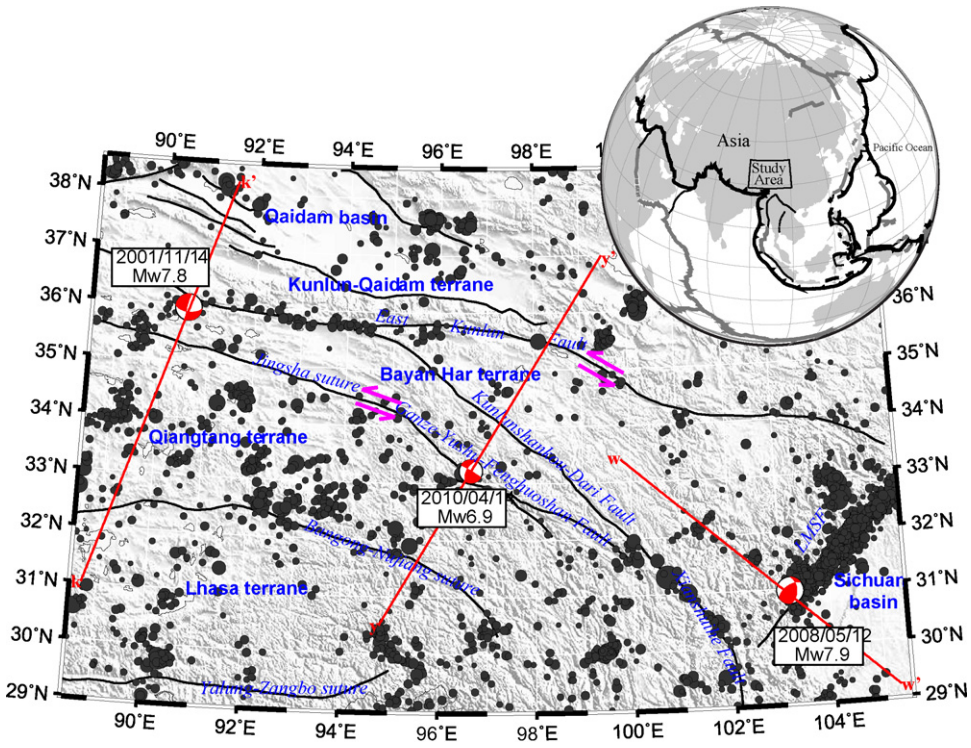

Fig. 1. Major geotectonic units in the NE Tibetan Plateau, and historic earthquakes with magnitudes bigger than 4.0 (black circles) since 1970. Beach balls indicate the focal mechanisms of the 2001 Kunlun, the 2008 Wenchuan, and the 2010 Yushu earthquakes. Pink arrows indicate the current direction of motion of the faults. Red lines are the locations of the S-wave velocity transects shown in Fig. 7. LMSF is the Longmen Shan Fault.

mated with the Qiangtang Terrane, which was to the south of it, during the late Triassic and early Jurassic (Dewey et al., 1988). In the Cenozoic, the Bayan Har Terrane, and indeed the entire Tibetan Plateau, was mainly influenced by the Indian–Eurasian collision. Since the Quaternary, the Longmen Shan Fault (Burchfiel et al., 1995; Densmore et al., 2007), the Ganze-Yushu-Fenghuoshan Fault (Xu et al., 2008), and the East Kunlun Fault (Zhou et al., 2009), all of which lie along the boundaries of Bayan Har Terrane, became seismically active.

To help us understand the present regional geodynamic environment, we construct a three-dimensional lithospheric S-wave velocity model for the NE Tibetan Plateau, by applying a regional surface-wave tomographic tool to a large amount of broad-band seismic data. We then proceed to extract deep-seated tectonic information, as revealed by the S-wave velocity structure, and then analyze the possible geodynamic settings that control the occurrence of strong earthquakes along the boundaries of the Bayan Har Terrane.

2. Regional surface-wave tomography

Surface-wave tomography is one of the preferred methods for exploring lithospheric structure because of its better vertical resolution in the lithosphere compared with teleseismic body-wave tomography. In most previous surface-wave tomographic studies, inversions of surface-wave dispersion measurements for a 3-D S-wave velocity model have been partitioned into two steps: period-by-period 2-D tomographic inversion for regionalized dispersion curves, and cell-by-cell inversion of regionalized dispersion curves for 1-D S-wave velocity profiles (e.g., Ritzwoller et al., 2002; Huang et al., 2003). This partitioned approach is not very efficient and cannot include 3-D *a priori* constraints to improve structure resolution, which may be one reason why previous regional studies on the Tibetan Plateau, using traditional surface-wave tomography (e.g., Su et al., 2002; Zhang et al., 2007), could not clearly delineate different tectonic terranes. Feng and An (2010) developed an efficient surface-wave tomographic method that combines the traditional partitioned two-step inversion equations into one formulation to directly invert surface-wave dispersion measurements for a 3-D S-wave velocity model. The method enables inclusion of 3-D *a priori* constraints, and of both regional (with both events and stations located within the study region) and teleseismic (with either epicenters or stations located outside the study region) measurements. The method has been successfully applied to continental-scale lithospheric studies of the Chinese mainland (Feng and An, 2010), and regional-scale studies of the North China Craton (An et al., 2009). We thus adopt the surface-wave tomographic method developed by Feng and An (2010) in the present study. A detailed description on the mathematic derivation of the methodology can be found in Feng and An (2010).

More and more temporary broad-band seismic arrays (e.g., INDEPTH and Hi-CLIMB) have been deployed in the hinterland of the Tibetan Plateau over the past years (e.g., Zhao et al., 1993; Nelson et al., 1996; Nabelek et al., 2005), and the results have provided important evidence for deep structures and the tectonic evolution of the regions near the seismic arrays (e.g., Kind et al., 2002; Wittlinger et al., 2009). However, most of the arrays have been arranged in a line, and the research results cannot properly cover the Tibetan Plateau in three-dimensions. Even so, as more seismic arrays are deployed, there has been an improvement in the lateral distribution of seismic stations on the plateau, which is essential for a 3-D tomographic study. For our work here, Rayleigh-wave group velocities are processed using a multiple filtering technique for these publicly open and non-publicly open seismic data, including those recorded by ~200 Hi-CLIMB (Nabelek et al., 2005) and ~50 INDEPTH-IV portable seismic stations (Zhao et al., 2008), and tens of permanent seismic stations belonging to the Yunnan and Sichuan Provincial Seismic Networks of China. In addition, we included the group-velocity data for China previously

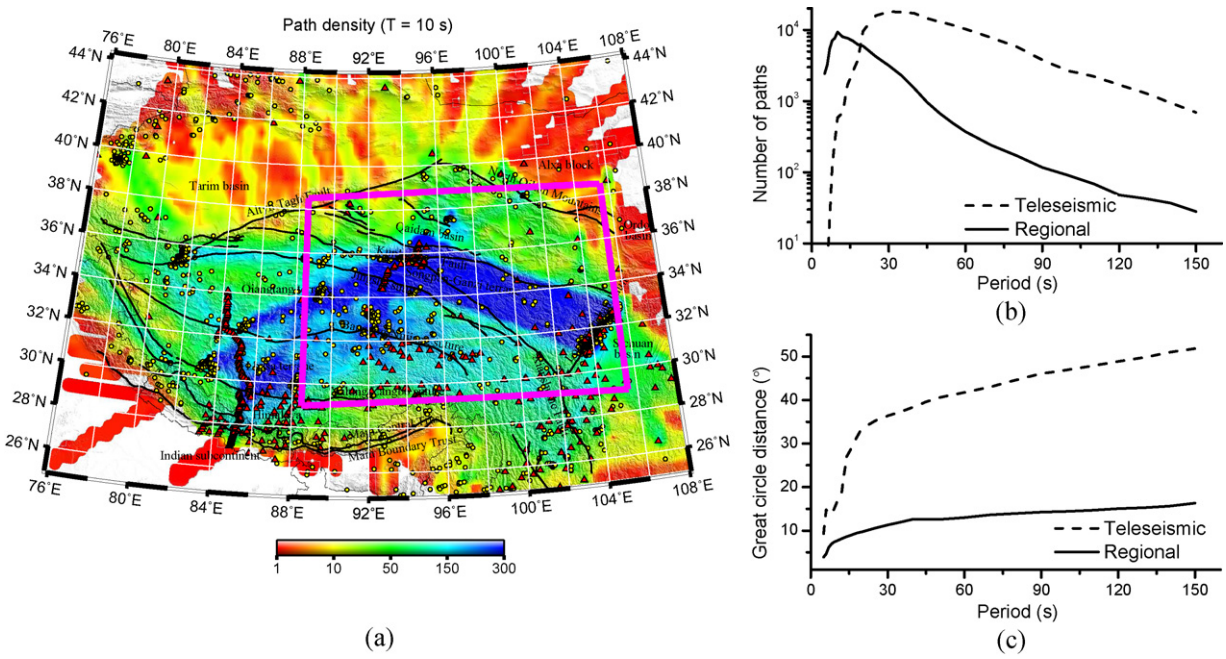

Fig. 2. Observational data showing (a) path density at period of 10 s, triangles and circles are seismic stations and epicenters within the study region, respectively; (b) the number of group-velocity measurements at different periods; and (c) the average epicentral distance at different periods. Solid lines in (b) and (c) (regional) represent data with rays completely within the study region, and dashed lines (teleseismic) represent data with rays partly within the study region.

processed by An et al. (2009) and Feng and An (2010). All these data form the best lateral data coverage to date for the Bayan Har Terrane and its surrounding regions. The seismic stations and events used in this study are shown in Fig. 2a as red triangles and yellow circles, respectively. The color image indicates the seismic-ray density at a period of 10 s, defined as the number of measurements intersecting each $0.4^\circ \times 0.4^\circ$ ($\sim$40 km $\times$ 44 km) area. The average ray density is better than $\sim$150 within most of the pink rectangle region.

According to the number of group-velocity measurements at different periods, we ultimately use group-velocity measurements at periods of 5–10 s with an interval of 1 s, at periods of 10–20 s with an interval of 2 s, at periods of 20–60 s with an interval of 5 s, and at periods of 60–150 s with an interval of 10 s. Fig. 2b and c respectively shows the total number of group-velocity measurements and average epicentral distances at different periods, where solid lines represent regional measurements with rays completely within the study region, and dashed lines represent teleseismic measurements with rays partly within the study region. At 10 s period, the number of regional group-velocity measurements is 9378 and the average epicentral distance is $\sim$7.6° ($\sim$800 km). The large content of short-period data will hopefully result in a better resolved lithospheric S-wave velocity model for the Bayan Har Terrane. According to the data coverage and period content of our surface-wave group-velocity measurements, we model an area as shown in Fig. 2a but limit our following discussion to the pink rectangle region where seismic ray density is good enough. The 3-D model is parameterized with a grid spacing of 0.4° in both longitude and latitude, and with a variable layer thickness in the vertical direction. The layer thickness is 5 km for depths less than 170 km, 10 km for depths from 170 to 250 km, and 50 km for depths from 250 to 300 km.

To decrease the degree of nonlinearity of surface-wave inversion for S-wave velocity, it is important to start from a 3-D reference model that is close to being realistic in the 3-D inversion. As the Moho is the sharpest discontinuity within the lithosphere and surface-waves are more sensitive to S-wave velocity than to a discontinuity, the primary consideration in constructing the 3-D reference model is crustal thickness or Moho depth below sea level rather than S-wave velocity. We thus collected/digitized point crustal thickness constraints from the published literature (Teng et al., 1983; Hirn et al., 1984; Cui et al., 1995; Zhao et al., 2001, 2006; Vergne et al., 2002; Wittlinger et al., 2004, 2009; Zhang and Klemperer, 2005; Li et al., 2006b; Liu et al., 2006, 2009; Shi et al., 2009; Wittlinger et al., 2009; Zhang et al., 2009; Mechie et al., 2011) and compiled a 3-D crustal thickness model for the study region (see Fig. 3). Crustal thickness for the INDEPTH-IV stations is estimated in the present study using the receiver function technique of Yuan et al. (1997). The grey and black circles in Fig. 3 denote locations where we have crustal thickness values from passive seismic receiver function studies and from controlled-source seismic studies, respectively. Regions without *a priori* point crustal thickness values are mainly constrained by the 3-D model of Li et al. (2006a) and by CRUST2.0 (Bassin et al., 2000). As to date there is no well established 3-D lithospheric S-wave velocity model for Tibet, we ultimately created the 3-D reference model by combining our compiled crustal-thickness model with the S-wave velocities of IASP91 (Kennett and Engdahl, 1991).

3. Model appraisal

The data fits between estimated and observed group velocities are qualitative indicators in evaluating the final inverted 3-D tomographic model. Fig. 4 shows four example dispersion-curve fits between observed and estimated group velocities. The dispersion curves estimated from the inverted model (solid lines) show a reasonable fit to the observed dispersion curves (triangles). Furthermore, as expected, the data fits of the inverted model are better than the fits of the reference model (dotted lines).

We routinely carried out checkerboard tests to show the spatial resolving power of the final model. To test lateral and vertical resolving power simultaneously, we set a 3-D synthetic model with horizontally- and vertically–alternating checkers. The input S-wave velocities were set as varying by ±7% relative to the reference model. As the surface waves of different periods have varying sensitivity and lateral resolution at different depths, we performed synthetic tests with three different checker sizes: $2^\circ \times 2^\circ \times 4$ layers

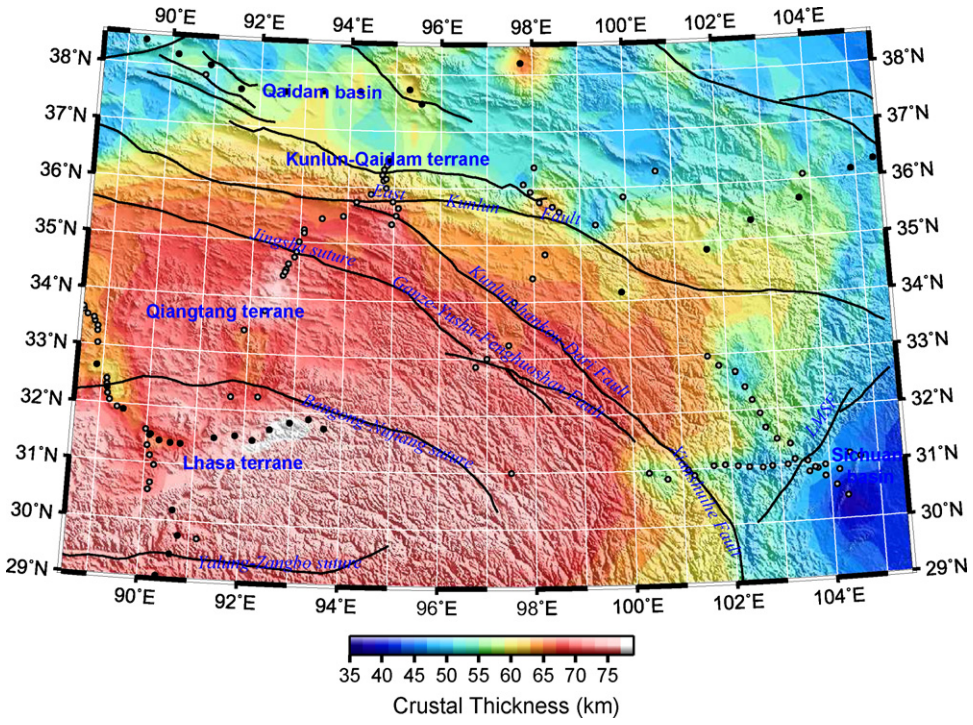

Fig. 3. Crustal thickness model compiled by the present study by collecting/digitizing point crustal thickness constraints from the published literature. The grey and black circles denote locations where we have crustal thickness values from passive seismic studies and from controlled-source seismic studies, respectively.

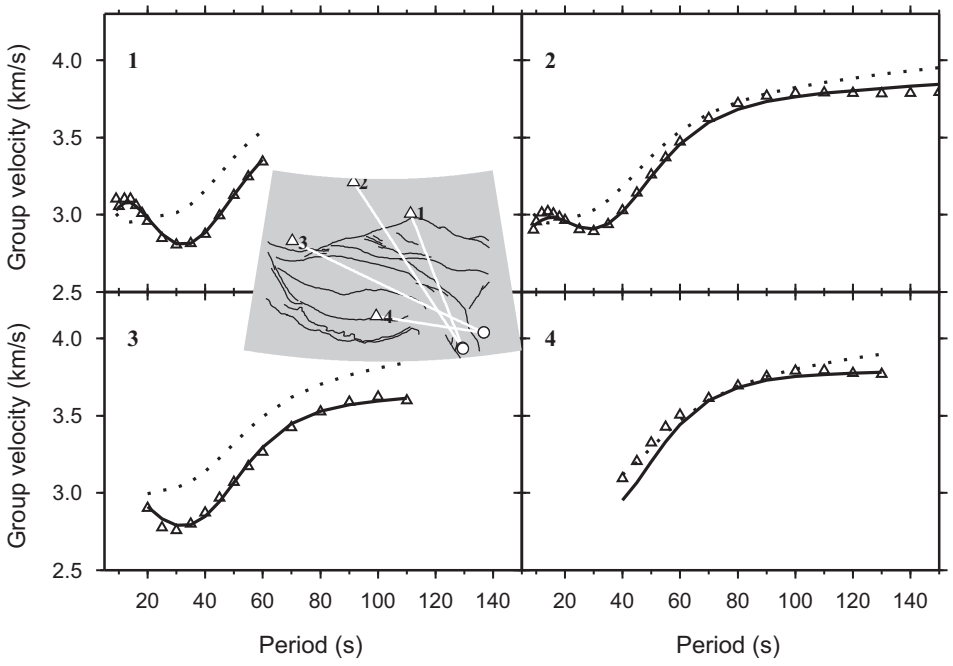

Fig. 4. Four example data fits between observed and predicted group-velocity dispersion curves. The dispersion curve number in the upper left of each frame corresponds to the ray path indicated by the same number in the inset map. Triangles denote observed dispersion curves, while solid and dotted lines represent predicted dispersion curves from the inverted S-wave velocity model and from the reference model, respectively. The inset map shows the paths, stations (triangles), and epicenters (circles) for the four dispersion curves.

in the x, y and z directions (~200 km × 222 km × 20 km; Fig. 5a), 3.2° × 3.2° × 6 layers (~320 km × 350 km × 30 km; Fig. 5b), and 4° × 4° × 14 layers (~400 km × 440 km × 70 km; Fig. 5c). Random noise was added to all the synthetic group-velocity measurements.

For most of the study region, the model retrieved 2° × 2° checkers down to 50 km depth, 3.2° × 3.2° checkers down to 70 km depth, and 4° × 4° checkers down to 200 km depth. Lebedev and Nolet (2003) suggested that the actual resolution is half of the recovered checker size. Therefore, the average lateral resolution length in the target study region is ~1° (~110 km) down to ~50 km depth, ~1.6° (~180 km) down to ~50 km, and ~2° (~220 km) down to ~200 km. Vertically, the average resolution is ~10 km down to ~50 km depth, ~15 km down to ~70 km and ~35 km down to ~200 km. The resolution decreases with depth and in marginal regions.

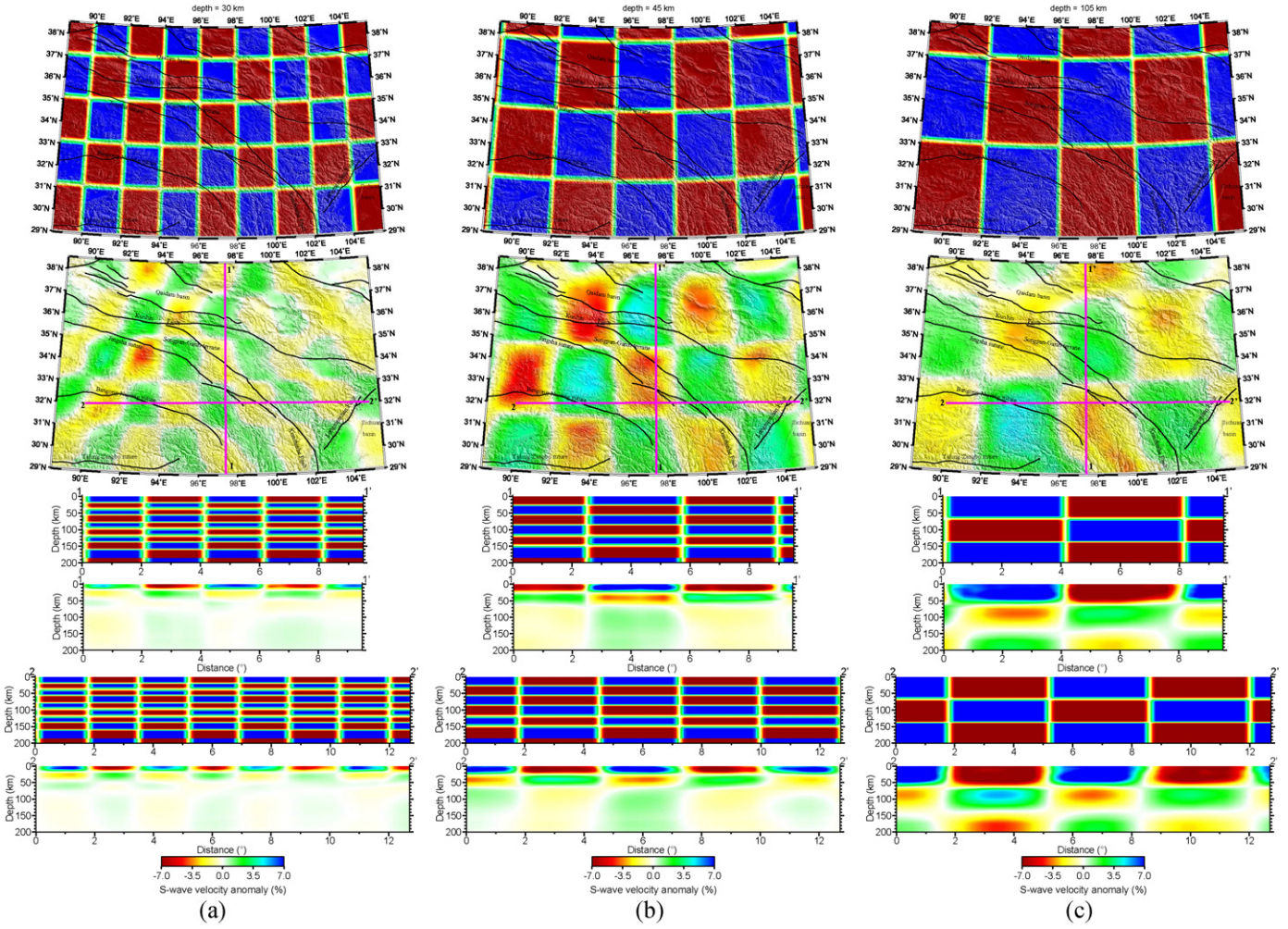

Fig. 5. Lateral and vertical S-wave velocity slices of the checkerboard test results. The sizes of 3-D checkers are (a) $2^\circ \times 2^\circ \times 4$ layers (longitude and latitude 2°; 4 layers vertically), (b) $3.2^\circ \times 3.2^\circ \times 6$ layers, and (c) $4^\circ \times 4^\circ \times 14$ layers. The odd rows show slices through the input model, and the even rows show slices through the retrieved model. The locations of vertical cross-sections are shown in the horizontal slices in the second row.

To test the resolving ability for realistic structures, we carried out hypothesis testing for a profile crossing through our study region. Fig. 6 shows the input and retrieved profiles of the hypothesis testing results. The structures of the input model (Fig. 6a) are set to be similar to the structures of our final inverted model on the same profile (to be shown in Fig. 7c). The retrieved model (Fig. 6b) recovers most of the structural features of the input model, including the thickness and depth extensions of the layers or plates, the gently dipping angle of the simulated Indian plate, the relative anomaly strength of the different plates (e.g., the Indian plate has a stronger positive anomaly than the paleo-Asian plate) and the approximate location of the low-to-high anomaly transition. As 3-D smoothing constraints have been applied in the tomographic inversion to stabilize the inversion, the low-to-high anomaly transition in the retrieved model becomes wider than in the input model, and the anomaly amplitude in the retrieved model is smaller than in the input model. However, the anomaly pattern of the input model is very well recovered by the retrieved model. We therefore believe that our dataset and inversion system is able to resolve structures down to ~200 km depth reliably.

4. S-wave velocity structures

Here, we extract three S-wave velocity transects which cross different parts of the NE Tibetan Plateau (Fig. 7, transect location shown in Fig. 1). The S-wave velocities derived from the surface-wave tomography are expressed as perturbations in percentages relative to the reference model.

Fig. 7a is a NE striking S-wave velocity transect (transect kk′) perpendicular to the north boundary of the Bayan Har Terrane, the East Kunlun Fault. From south to north, the profile crosses through the Lhasa, Qiangtang, Bayan Har, and Kunlun-Qaidam terranes. At the top of the transect is exaggerated topography. The transect is generally dominated by low velocities (warm colors). At depths of ~110–200 km (beneath the pink dashed line in Fig. 7a), the Lhasa, southern Qiangtang, and Kunlun-Qaidam terranes have higher velocities than the northern Qiangtang and Bayan Har terranes. The relatively high velocity beneath the Lhasa and southern Qiangtang terranes extends in a nearly horizontal direction, possibly reflecting the front of the Indian Plate as it subducts beneath the plateau, while the relatively high velocity beneath the Kunlun-Qaidam terrane possibly reflects the paleo-Asian lithosphere. The northern Qiangtang and Bayan Har terranes are characterized by very low velocities, and are bordered by the above mentioned two areas of relatively high velocity. Along the INDEPTH-III seismic profile, Tilmann et al. (2003) imaged such strong low upper-mantle velocities beneath the Qiangtang terrane in their teleseismic tomographic study and correlated them to an upwelling. As our regional model only covers depths above 200 km and the low-velocity area extends not as a narrow belt but is very wide, we prefer correlating the low velocity with a gap or high-temperature extrusions between the converging Indian and Asian lithospheres (Feng et al.,

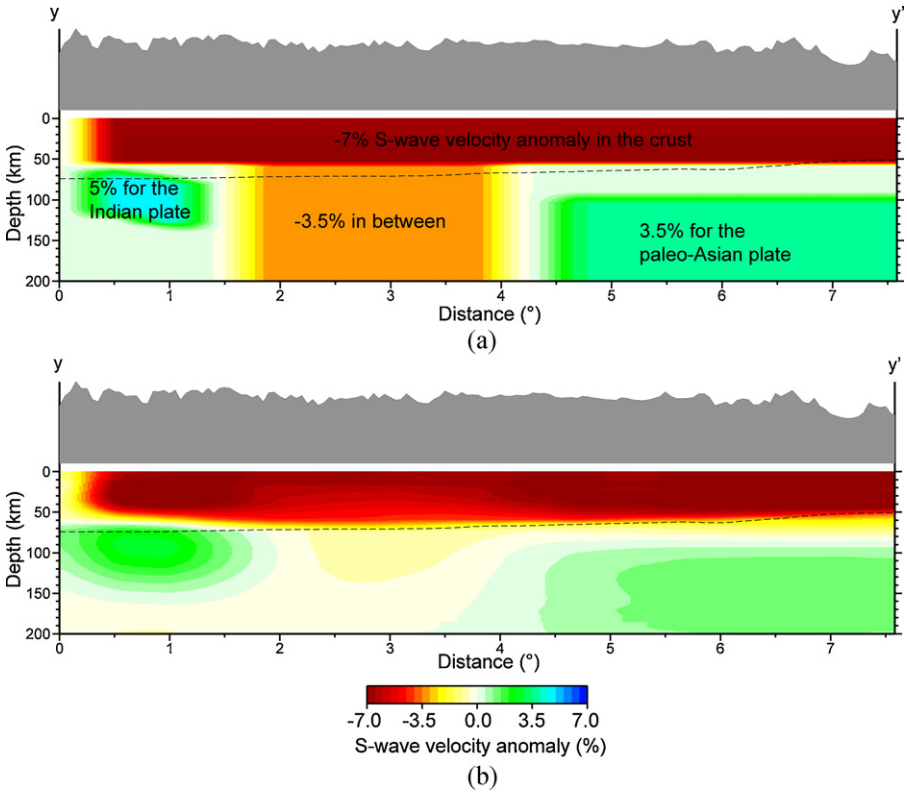

Fig. 6. Input (a) and retrieved structures (b) of hypothesis testing for a profile crossing the Ganze-Yushu-Fenghuoshan Fault (profile yy′, location is shown in Fig. 1).

2010). The Kunlun earthquake occurred above a low-velocity crust and upper mantle (Fig. 7a).

Fig. 7b is a NW striking S-wave velocity transect (transect ww') perpendicular to the east boundary of the Bayan Har Terrane, the Longmen Shan Fault. This transect mainly crosses the eastern Bayan Har Terrane and the Sichuan Basin. The topography varies markedly across the Longmen Shan Fault. Both the crust and the upper-mantle lithosphere have strong lateral velocity variations. The Bayan Har Terrane, northwest of the Longmen Shan Fault, has a low-velocity layer above ~150 km, and a weak high-velocity layer underneath. For the Sichuan Basin, both the crust and upper-mantle lithosphere show marked high velocities, except for the shallow low-velocity sedimentary layer. The Wenchuan earthquake occurred on the transition zone between the low-velocity Bayan Har Terrane and the high-velocity Yangtze Craton (Fig. 7b).

Fig. 7c is a NE striking S-wave velocity transect (transect yy′) perpendicular to the west boundary of the Bayan Har Terrane, the Ganze-Yushu-Fenghuoshan Fault. The lateral variation of upper-mantle lithospheric velocity is similar to that shown in transect kk′ (Fig. 7a). The Lhasa, Bayan Har, and Kunlun-Qaidam terranes have high upper-mantle lithospheric velocities, whereas in between is a distinctive low-velocity zone below the Qiangtang Terrane. The weakly northward-dipping high velocity zone beneath the Lhasa terrane may represent the subducting Indian lithosphere beneath the Tibetan plateau. The wide horizontal extent of the high velocity zone beneath the Bayan Har and Kunlun-Qaidam terranes may reflect the paleo-Asian lithosphere. The low velocity zone in between may represent the high-temperature extrusions/partial melts caused by the converging Indian and Asian lithospheres. The Yushu earthquake occurred above a low-velocity crust and upper mantle (Fig. 7c). This transect partly overlaps with profile J in the teleseismic body-wave study of Li et al. (2008). Our transect yy′ images the subducting Indian Plate much further to the north than shown in profile J of Li et al. (2008). The difference may be caused by the different data types used and different resolution lengths provided at lithospheric depths by teleseismic body-wave tomography and regional surface-wave tomography. In contrast, besides showing more detailed structures, our regional surface-wave tomographic model images a similar northward extension of the Indian Plate and similar long wavelength structures to the global surface-wave tomographic model of Lebedev and Van der Hilst (2008) in the same area, confirming the robustness and reliability of our regional surface-wave tomographic model.

Another common feature shown both on transect kk′ and transect yy′ is that a weak velocity discontinuity at ~110 km depth (marked as pink dashes in Fig. 7a and c) seems to exist, which separates the Tibetan upper-mantle lithosphere into two distinct layers.

5. Discussion

5.1. Stacking of the Tibetan lithospheres

Lithospheric mantle is generally characterized by high velocities compared with the overlying low-velocity crust and underlying asthenosphere, so a qualitative analysis of thickness or geometry of the lithospheric mantle beneath the study region can be carried out based on our S-wave velocity anomaly at uppermost mantle depths. High or relatively high velocities at the south-western ends of profiles kk′ and yy′ (beneath central-south Tibet) extend down to at least 170–200 km, indicating a very thick lithosphere of at least 170–200 km in central-south Tibet. A wide region of low-velocities between the Bangong-Nujiang-Suture (BNS) and the Bayan Har terrane on profiles kk′ and yy′ implies a strongly thinned lithosphere in central-north Tibet. High or relatively high velocities down to ~200 km appear again beneath the Kunlun-Qaidam terrane on profiles kk′ and yy′, implying that the lithosphere thickness increases again beneath the Kunlun-Qaidam terrane. Jiménez-Munt et al. (2008) have made a dynamic model of the Himalayas based on topography, gravity, geoid and heat flow data along a 2D

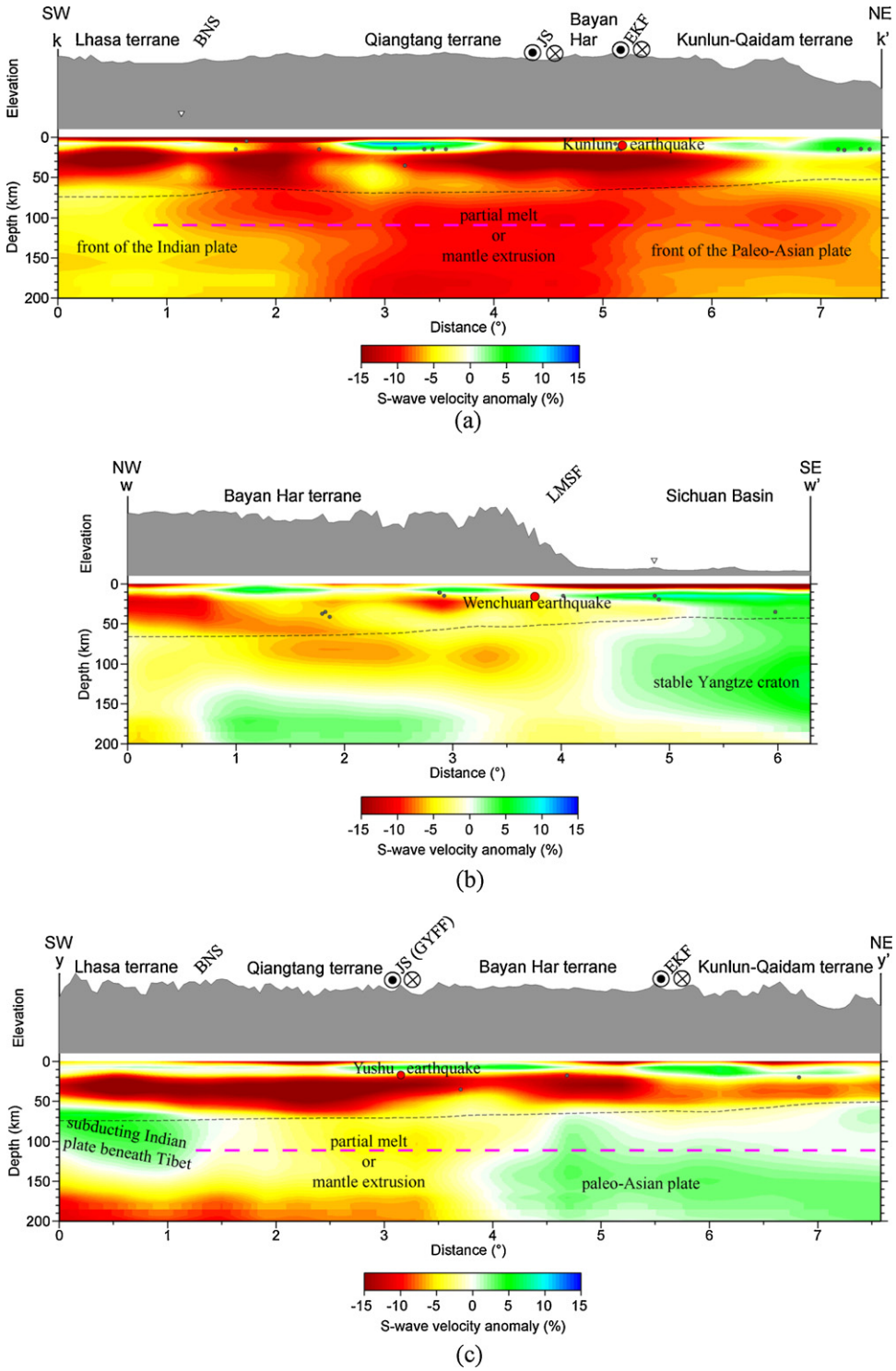

Fig. 7. S-wave velocity transects across different parts of the NE Tibetan Plateau. (a) Profile kk′ crossing the East Kunlun Fault; (b) profile ww′ crossing the Longmen Shan Fault; and (c) profile yy′ crossing the Ganze-Yushu-Fenghuoshan Fault. The top of each transect shows exaggerated topography; small black circles are historic earthquakes; black dashes are Moho depths from the 3-D reference model; BNS – Bangong-Nujiang Suture; JS – Jingsha suture; EKF – East Kunlun Fault; LMSF – Longmen Shan Fault; GYFF – Ganze-Yushu-Fenghuoshan Fault.

cross-section that is located between our profiles k–k′and y–y′. In their dynamic model, the lithosphere reaches a maximum depth of ~260 km beneath the southern Plateau (not covered by our study region), and thins abruptly northward to ~100 km under the central and northern Plateau. The lithospheric thickness increases again beneath the Qaidam basin and Qilian Shan to ~160 km. The tendency of the lithospheric thickness variations across the Tibetan Plateau indicated by our S-wave velocities is well consistent with the dynamic model of Jiménez-Munt et al. (2008).

Normally, the thickness of non-cratonic lithosphere (~100 km) is smaller than cratonic lithosphere (150–250 km) (An and Shi, 2006). The Tibetan Plateau is of a non-cratonic nature. However, transects kk′ and yy′ (Fig. 7a and c) both exhibit relatively high or high upper-mantle lithospheric velocities down to 160–200 km

beneath the Lhasa and Kunlun-Qaidam terranes, suggesting a lithosphere as thick as that for a craton, and confirming that the thickness of the lithosphere beneath Tibet is ~160–220 km (An and Shi, 2006). Previous studies (e.g., Feng et al., 2010) have proposed that the southern Tibetan lithosphere may be thickened due to a doubling of the subducting Indian Plate, but they did not explain the lithosphere thickening in the NE Tibetan Plateau. If the Tibetan lithosphere was really thickened, it is still unclear which part of the lithosphere pertains to the plateau itself, and which part is due to tectonic emplacement.

In our model, the upper-mantle lithospheric S-wave velocities above ~110 km, as for example on transects kk′ and yy′, are seemingly different from the velocities below ~110 km. This structural feature may suggest that though the lithosphere of the Tibetan plateau is as thick as ~160–220 km (An and Shi, 2006), the original lithosphere of the plateau could be not thicker than ~110 km and the part below could be assigned to the emplaced Indian slab in the southern plateau or others in the northeastern plateau. According to this interpretation, for the stacked lithosphere with a thickness of ~160–220 km, after subtracting the overlying ~110 km original lithosphere of the plateau, the emplaced lithosphere should be ~50–110 km thick, which is also a reasonable thickness for typical upper-mantle lithosphere (not including crustal thickness).

For the southern Tibetan Plateau (the Lhasa and southern Qiangtang terranes in Fig. 7a and c), it is easy to understand that the lithospheric stacking/doubling is caused by the subduction of Indian lithosphere, as previously proposed by Feng et al. (2010). However, for the northeastern plateau, there remains difficulty to clarify the cause of the lithosphere thickening. To understand better the possible evolution of the NE Tibetan Plateau, we propose the possible dynamic process as shown by the cartoons in Fig. 8. Fig. 8a is a simplified model for the NE Tibetan Plateau based on the structural image of Fig. 7c. For the northeastern plateau, some researchers believe that the Kunlun-Qaidam Terrane has subducted southwards, along the Kunlun suture zone, from the late to middle Miocene (Tapponnier et al., 2001; Kind et al., 2002), as illustrated by "model 1" in Fig. 8b. If so, the lithospheric thickening beneath the Bayan Har terrane south of the East Kunlun Fault (Fig. 7c) may be caused by this southward Kunlun-Qaidam subduction. However, this model cannot explain the thickened lithosphere beneath the Kunlun-Qaidam terrane itself.

Alternatively, if the Kunlun-Qaidam terrane never underwent southwards subduction, the lithospheric thickening beneath the northeastern Tibetan Plateau could be related to the pre-existing paleo-Asian lithosphere, as shown by "model 2" in Fig. 8b. Since the Late Mesozoic, the Qaidam Basin has been separated from the Tarim Basin (Ge and Liu, 2000) and has then moved northeastwards with a distance of several hundred kilometers during the Indian–Eurasian collision/post-collision. More specifically, the Kunlun-Qaidam terrane has been deformed by northeastwards push transferred from the Bayan Har Terrane south of it. If the pre-existing paleo-Asian lithosphere had a stable and thick lithosphere root (e.g., ~200 km), the northeastward push transferred by the thinner Kunlun-Qaidam lithosphere (~110 km thick) would only be able to move northeastwards the upper part of the paleo-Asian lithosphere (above ~110 km), while the root of the paleo-Asian lithosphere (depth below ~110 km) would have been left, unmoved ("model 2" in Fig. 8b). In this way, an unmoved, pre-existing lithospheric root of the paleo-Asian Plate could be responsible for the stacking of the lithosphere beneath the northeastern Tibetan Plateau.

Furthermore, in the convergent movement indicated by "model 2", the Kunlun-Qaidam terrane may also overthrust the paleo-Asian plate as illustrated by "model 3" in Fig. 8b. Both "model 2" and "model 3" could finally result in the present structural image with thickened lithosphere in the NE Tibetan Plateau.

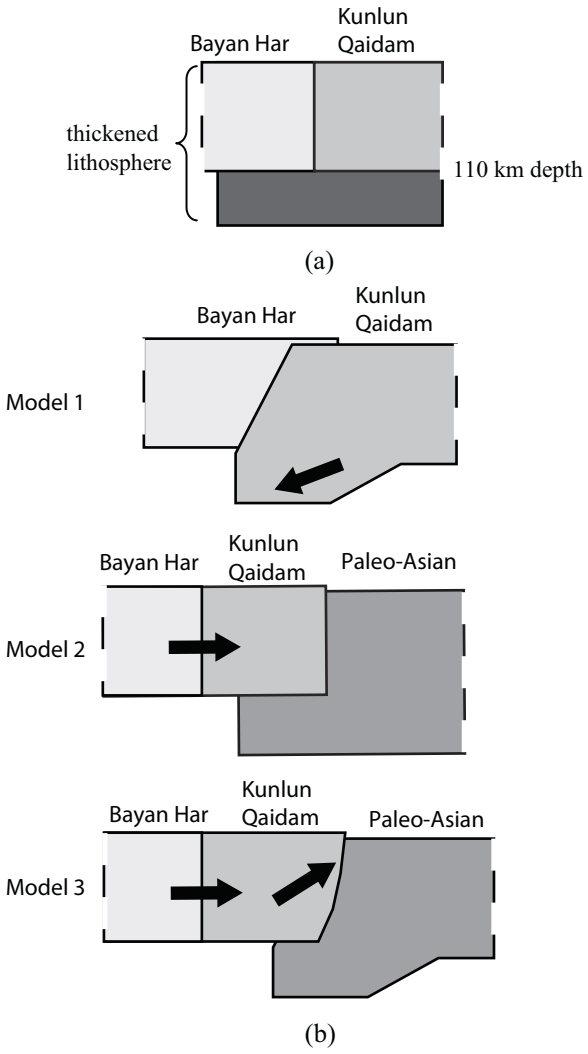

Fig. 8. Cartoons to illustrate possible dynamic processes involved in the evolution of the NE Tibetan Plateau. (a) Simplified model according to Fig. 7c. (b) Three possible dynamic models. See text for further discussion.

In summary, the deep structure of the northeastern Tibetan Plateau (including the Bayan Har Terrane and its surrounding regions) are not only controlled by the northwards subduction of the Indian Plate, as previously proposed by many researchers, but possibly also by pre-existing remnants of the paleo-Asian lithosphere.

5.2. Lithospheric structures and seismogenic environment of strong earthquakes

Fig. 9a and b shows horizontal slices of velocities at 15 and 120 km depths, and earthquakes of magnitude bigger than 5.0 since 1962 (from www.GlobalCMT.org) with well-determined focal mechanisms (colored circles). The short bar across the circles indicates the horizontal projection of the *P*-axis, as indicated by the focal mechanism solution. Fig. 9a shows a poor correlation between seismicity and crustal velocity anomalies, though most earthquakes in the Tibetan Plateau occur in the shallow crust. In comparison, Fig. 9b shows a general correlation between seismicity (also refer to Fig. 1 for earthquakes with magnitudes of 4.0–5.0) and upper-mantle lithospheric velocity anomalies. The western Bayan Har Terrane, with low upper-mantle lithospheric velocities, is seismically more active than the eastern part of the terrane, which has

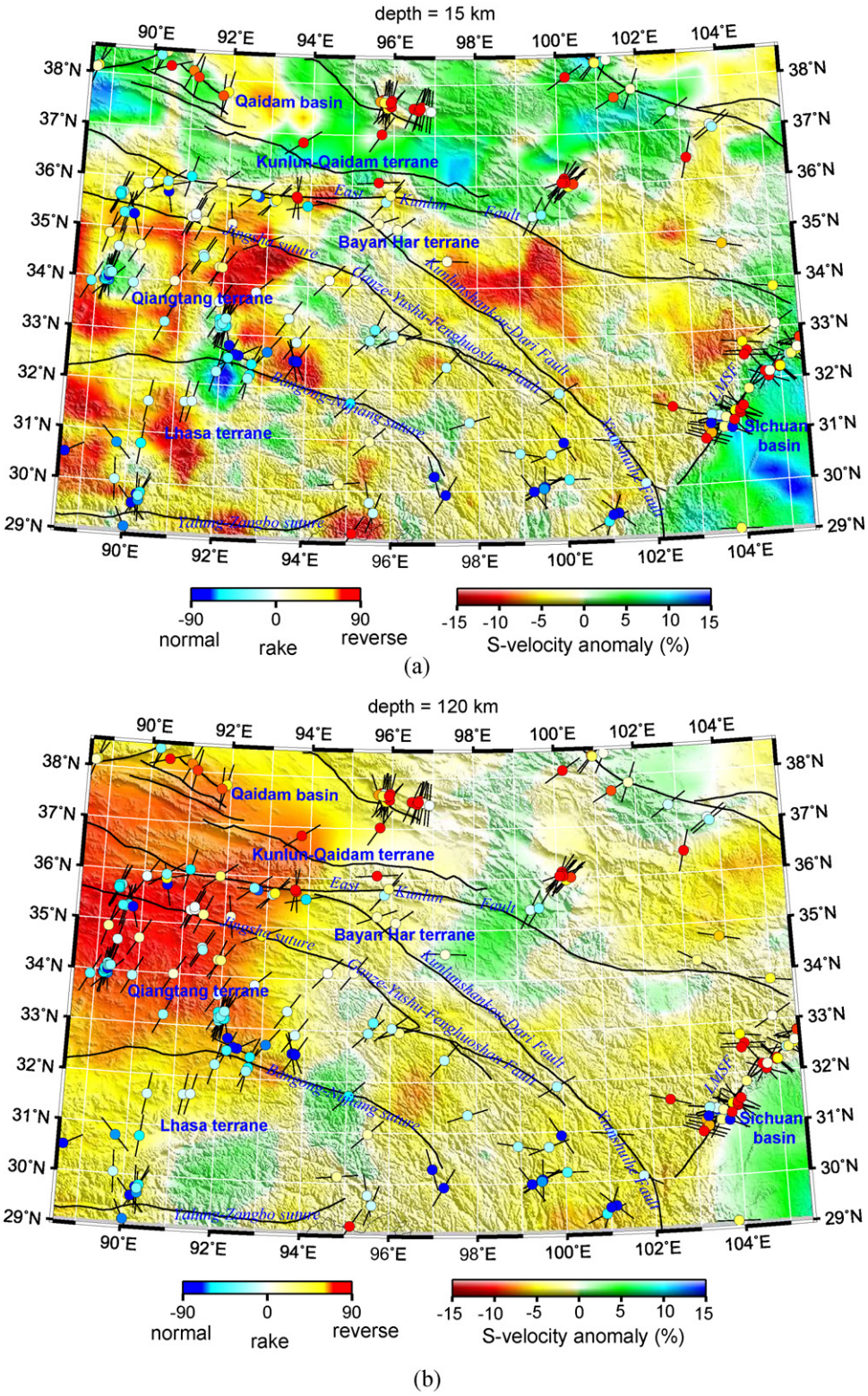

Fig. 9. Horizontal sections showing lithospheric S-wave velocity at the depths of (a) 15 and (b) 120 km and earthquakes of magnitudes bigger than 5.0 since 1962 with well-determined focal mechanisms (colored circles). The short bars across the circles indicate the horizontal projection of the *P*-axis from the focal mechanism solution.

high velocities. Similarly, the western Qiangtang Terrane, dominated by distinctly low velocities in the upper-mantle lithosphere, is seismically more active than the Lhasa and Kunlun-Qaidam terranes to the south and north of it. The correlation may confirm that weak or ductile upper-mantle lithosphere, with low velocities, is easier to deform than strong or brittle upper-mantle lithosphere with high velocities. Furthermore, Fig. 9b shows that faults in the low-velocity region in upper-mantle lithosphere are normally characterized by normal (extension) to strike-slip movements (circles shaded with cool colors), while reverse fault movements (compression), sometimes with a small strike-slip component (circles shaded with warm colors), normally occur in the low-to-high

velocity transition zone of the upper-mantle lithosphere. The correlation of seismicity and fault activity with upper-mantle lithospheric velocity anomalies suggests that the strength (mechanical property) of the upper-mantle lithosphere not only has an influence on the intensity of seismicity but also has a correlation with the deformation mode of the overlying crust.

The Wenchuan earthquake occurred on the primary tectonic boundary between the Tibetan Plateau and the South China block, and also within the transition zone between the low-velocity eastern Bayan Har Terrane and the high-velocity Yangtze Craton in the lithospheric upper mantle. The Wenchuan earthquake resulted from thrusting with a dextral strike-slip component, and was considered to be the result of resistance from the stable Yangtze Craton to the uplift and eastwards expansion of the Tibetan Plateau (e.g., Burchfiel et al., 2008; Dong et al., 2008; An et al., 2010). In comparison, the Kunlun and Yushu earthquakes resulted from strike-slip movements along boundary faults inside the Tibetan Plateau. Both have similar deep tectonic settings, and both are located above regions with low velocities in the upper-mantle lithosphere. South and north of the epicentral regions of the earthquakes, the images presented here show relatively high or high velocities in the upper-mantle lithosphere that correlate with the Indian and Asian lithospheres, respectively. This suggests that the Kunlun and Yushu earthquakes may be related to the convergence of the Indian and Asian lithospheres.

The Wenchuan and Kunlun earthquakes have a different character of fault activity, suggesting that they have different geodynamic settings. In the eastern plateau, the eastern Bayan Har Terrane and the Sichuan Basin, separated by the Longmen Shan Fault, have large velocity contrasts in the upper-mantle lithosphere (Fig. 7b). Due to the thick, high-velocity, cold lithosphere of the Yangtze Craton strongly resisting ("braking") the expansion of the Tibetan Plateau, the "brake belt" (Longmen Shan Fault belt) is confined within a very narrow belt of tens of kilometers. However, in the northern plateau, the western Bayan Har Terrane and the Qaidam Basin, separated by the East Kunlun Fault, have only a weak velocity contrast in their upper-mantle lithosphere (Fig. 7a), suggesting that the Qaidam Basin does not have the same stable lithospheric root as the Sichuan Basin. Therefore, the Qaidam Basin is not able to "brake" the expansion of the northern plateau. The wide distribution of thrust activity (warm color circles in Fig. 9b), north of the East Kunlun Fault, also confirms that the weak resistance of the Kunlun-Qaidam Terrane to the expansion of the northern Tibetan Plateau has not been concentrated in a narrow brake-like belt but is dispersed over a wide area. The weak resistance of the Kunlun-Qaidam Terrane could be the reason why the Qaidam Basin has been separated from the Tarim Basin since the Late Mesozoic (Ge and Liu, 2000), and has been displaced northwards to its present location. In the interior of the Tibetan Plateau, because of the relative stability within any one tectonic block, it is strike-slip activity along boundary faults between the blocks that has played an important role in adjusting and balancing the deformation caused by the uplift and expansion of the plateau (Tapponnier et al., 2001). The Kunlun and Yushu earthquakes are just two events that resulted from such strike-slip fault movements along the boundaries of blocks in the interior of the plateau. Therefore, they are both the result of deformation adjustment occurring within the tectonic blocks in the Tibetan plateau, and thus can promote the eastwards extrusion of the plateau.

6. Conclusions

A well-constrained three dimensional lithospheric S-wave velocity model for the NE Tibetan Plateau was constructed using a regional surface-wave tomographic tool. The velocity model imaged an abnormally thick (~160–200 km) lithosphere beneath the Tibetan Plateau. A weak velocity discontinuity is present at ~110 km depth that seemingly separates the thick Tibetan upper-mantle lithosphere into two layers. We thus proposed that the upper layer of the Tibetan lithosphere (above ~110 km) may pertain to the plateau itself while the lower layer of the lithosphere (below ~110 km) may come from the subducting Indian plate (in the southern plateau) or from the pre-existing remnant of the paleo-Asian plate (in the northeastern plateau).

Furthermore, the upper-mantle lithospheric velocity structures correlate in various ways with seismicity and the type of fault involved. Regions with low velocities in the upper-mantle lithosphere have a stronger seismicity than regions with high velocities. This is to be expected because the low-velocity lithosphere is weaker than the high-velocity lithosphere, and is thus more easily deformed. The fault movements associated with low velocity upper-mantle lithosphere are typically normal or strike-slip, while the faults associated with the low-to-high velocity transition zone are thrusts, sometimes with a small strike-slip component. The 2001 Mw 7.8 Kunlun and 2010 Mw 6.9 Yushu earthquakes were the result of strike-slip fault activities occurring within the bounds of the low velocity region in the upper-mantle lithosphere (weak lithosphere). The 2008 Mw 7.9 Wenchuan earthquake was the result of oblique reverse fault movement in the transition zone between the low-velocity eastern Bayan Har Terrane and the high-velocity Yangtze Craton. Though most earthquakes on the Tibetan Plateau are the result of crustal fault movements, the correlation between seismicity and upper-mantle lithospheric velocity suggests that the strength (mechanical or rheological properties) of the upper-mantle lithosphere can influence the mode of deformation of the overlying crust.

Acknowledgements

This work was mainly supported by the Basic Research Foundation of the Institute of Geomechanics, Chinese Academy of Geological Sciences (No. DZLXJK201003). The INDEPTH-IV passive seismic data were collected with the joint support of the China Geological Survey (grant 21212010511809) and the Deutsche Forschungsgemeinschaft and the Deutsches GeoForschungsZentrum – GFZ, Potsdam in Germany. The instruments for the INDEPTH-IV passive seismic experiment were provided by the Geophysical Instrument Pool of the Deutsches GeoForschungsZentrum – GFZ, Potsdam (GIPP), Germany and SEIS-UK. We are also grateful to the China Earthquake Data Center and IRIS for making available some seismic data we analyzed during our study. Figures were generated using Generic Mapping Tools (Wessel and Smith, 1991).

References

An, M., Feng, M., Long, C., 2010. Deep ruptures around the hypocenter of the 12 May 2008 Wenchuan Earthquake deduced from aftershock observations. Tectonophysics 491 (1–4), 96–104.
An, M., Feng, M., Zhao, Y., 2009. Destruction of lithosphere within the north China craton inferred from surface wave tomography. Geochem. Geophys. Geosyst. 10 (8), Q08016.
An, M., Shi, Y., 2006. Lithospheric thickness of the Chinese continent. Phys. Earth Planet. In. 159, 257–266.
Bassin, C., Laske, G., Masters, G., 2000. The current limits of resolution for surface wave tomography in North America. EOS Trans. AGU 81, F897.
Burchfiel, B., Chen, Z., Liu, Y., Royden, L., 1995. Tectonics of the Longmen Shan and adjacent regions, central China. Int. Geol. Rev. 37, 661–735.
Burchfiel, B.C., Royden, L.H., van der Hilst, R.D., Hager, B.H., Chen, Z., King, R.W., Li, C., Lü, J., Yao, H., Kirby, E., 2008. A geological and geophysical context for the Wenchuan earthquake of 12 May 2008, Sichuan, People's Republic of China. GSA Today 18 (7), 4–11.
Cui, Z.-z., Li, Q.-s., Wu, C.-d., Yin, Z.-x., Liu, H.-b., 1995. The crustal and deep structures in Golmud-Ejin Qi GGT. Acta Geophys. Sinica 38, 15–28.

Densmore, A.L., Ellis, M.A., Li, Y., Zhou, R., Hancock, G.S., Richardson, N., 2007. Active tectonics of the Beichuan and Pengguan faults at the eastern margin of the Tibetan Plateau. Tectonics 26, TC4005.
Dewey, J.F., Shackleton, R.M., Chengfa, C., Yiyin, S., 1988. The tectonic evolution of the Tibetan Plateau. Philos. Trans. Roy. Soc. London A: Math. Phys. Sci. 327 (1594), 379–413.
Dong, S., Zhang, Y., Long, C., Wu, Z., An, M., Zhang, Y., Yang, N., Chen, Z., Lei, W., Shi, W., Shi, J., 2008. Surface rupture investigation of the Wenchuan Ms 8.0 earthquake of May 12th, 2008, West Sichuan, and analysis of its occurrence setting. Acta Geosci. Sinica 29 (3), 392–396.
Feng, M., An, M., 2010. Lithospheric structure of the Chinese mainland determined from joint inversion of regional and teleseismic Rayleigh-wave group velocities. J. Geophys. Res. 115, B06317.
Feng, M., van der Lee, S., An, M., Zhao, Y., 2010. Lithospheric thickness, thinning, subduction, and interaction with the asthenosphere beneath China from the joint inversion of seismic S-wave train fits and Rayleigh-wave dispersion curves. Lithos, doi:10.1016/j.lithos.2009.11.017.
Ge, X., Liu, J., 2000. Broken Western China Craton. Acta Petrol. Sinica 16 (1), 59–66.
Hirn, A., Lepine, J.-C., Jobert, G., Sapin, M., Wittlinger, G., Xin, X.Z., Yuan, G.E., Jing, W.X., Wen, T.J., Bai, X.S., Pandey, M.R., Tater, J.M., 1984. Crustal structure and variability of the Himalayan border of Tibet. Nature 307, 23–25.
Huang, Z., Su, W., Peng, Y., Zheng, Y., Li, H., 2003. Rayleigh wave tomography of China and adjacent regions. J. Geophys. Res. 108 (B2), 2073.
Jiménez-Munt, I., Fernàndez, M., Vergés, J., Platt, J.P., 2008. Lithosphere structure underneath the Tibetan Plateau inferred from elevation, gravity and geoid anomalies. Earth Planet. Sci. Lett. 267, 276–289.
Kennett, B.L.N., Engdahl, E.R., 1991. Traveltimes for global earthquake location and phase identification. Geophys. J. Int. 105, 429–465.
Kind, R., Yuan, X., Saul, J., Nelson, D., Sobolev, V., Mechie, S., Zhao, J., Kosarev, W., Ni, G., Achauer, J., Jiang, U.M., 2002. Seismic images of crust and upper mantle beneath Tibet: evidence for Eurasian plate subduction. Science 298, 1219–1221.
Lebedev, S., Nolet, G., 2003. Upper mantle beneath Southeast Asia from S velocity tomography. J. Geophys. Res. 108 (B1), 2048.
Lebedev, S., Van der Hilst, R.D., 2008. Global upper-mantle tomography with the automated multi-mode surface and S waveforms. Geophys. J. Int. 173 (2), 505–518.
Li, C., van der Hilst, R.D., Meltzer, A.S., Engdahl, E.R., 2008. Subduction of the Indian lithosphere beneath the Tibetan Plateau and Burma. Earth Planet. Sci. Lett. 274, 157–168.
Li, S.L., Mooney, W.D., Fan, J.C., 2006a. Crustal structure of mainland China from deep seismic sounding data. Tectonophysics 420, 239–252.
Li, Y.H., Tian, X.B., Wu, Q.J., Zeng, R.S., Zhang, R.Q., 2006b. The Poisson ratio and crustal structure of the central Qinghai-Xizang inferred from INDEPTH-III teleseismic waveforms: geological and geophysical implications. Chinese J. Geophys. 49 (4), 1037–1044.
Lin, A., Fu, B., Guo, J., Zeng, Q., Dang, G., He, W., Zhao, Y., 2002. Co-seismic strike-slip and rupture length produced by the 2001 Ms 8.1 central Kunlun earthquake. Science 296, 2015–2017.
Liu, M., Mooney, W.D., Li, S., Okaya, N., Detweiler, S., 2006. Crustal structure of the northeastern margin of the Tibetan plateau from the Songpan-Ganzi terrane to the Ordos basin. Tectonophysics 420, 253–266.
Liu, Q.Y., Li, Y., Chen, J.H., Guo, B., Li, S.C., Wang, J., Zhang, X.Q., Qi, S.H., 2009. Wenchuan Ms8.0 earthquake: preliminary study of the S-wave velocity structure of the crust and upper mantle. Chinese J. Geophys. 52 (2), 309–319.
Mechie, J., Kind, R., Saul, J., 2011. The seismological structure of the Tibetan Plateau crust and mantle down to 700 km depth. In: Gloaguen, R., Ratschbacher, L. (Eds.), Growth and Collapse of the Tibetan Plateau. Geological Society of London, London, pp. 109–125.
Nabelek, J., Vergne, J., Hetenyi, G., Hi-CLIMB team, 2005. Project Hi-CLIMB: a synoptic view of the Himalayan Collision Zone and Southern Tibet. EOS Trans. AGU 86 (52), Abstract T52A-02.
Nelson, K.D., Zhao, W., Brown, L.D., Kuo, J., Che, J., Liu, X., Klemperer, S.L., Makovsky, Y., Meissner, R., Mechie, J., Kind, R., Wenzel, F., Ni, J., Nabelek, J., Leshou, C., Tan, H., Wei, W., Jones, A.G., Booker, J.U., Kidd, M., Hauck, W.S.F., Alsdorf, M., Ross, D., Cogan, A., Wu, M., Sandvol, C., Edwards, E.M., 1996. Partially molten middle crust beneath southern Tibet: synthesis of project INDEPTH results. Science 274, 1684–1688.
Ritzwoller, M.H., Shapiro, N.M., Barmin, M.P., Levshin, A.L., 2002. Global surface wave diffraction tomography. J. Geophys. Res. 107 (B12), 2335.
Shi, D., Shen, Y., Zhao, W., Li, A., 2009. Seismic evidence for a Moho offset and south-directed thrust at the easternmost Qaidam-Kunlun boundary in the Northeast Tibetan plateau. Earth Planet. Sci. Lett. 288, 329–334.
Su, W., Peng, Y., Zheng, Y., Huang, Z., 2002. Crust and upper mantle shear velocity structure beneath the Tibetan Plateau and adjacent areas. ACTA Geoscientia Sinica 23 (3), 193–200.
Tapponnier, P., Xu, Z., Roger, F., Meyer, B., Arnaud, N., Wittlinger, G., Yang, J., 2001. Oblique stepwise rise and growth of the Tibetan Plateau. Science 294 (5547), 1671–1677.
Teng, J.-W., Sun, K.-Z., Xiong, S.-B., Yin, Z.-X., Yao, H., Chen, L.-F., 1983. Deep seismic reflection waves and structure of the crust from Dangxung to Yadong on the Xizang Plateau (Tibet). Phys. Earth Planet. Ints. 31, 293–306.
Tilmann, F., Ni, J., INDEPTH III Seismic Team, 2003. Seismic imaging of the downwelling Indian lithosphere beneath central Tibet. Science 300, 1424–1427.
Vergne, J., Wittlinger, G., Qiang, H., Tapponnier, P., Poupinet, G., Jiang, M., Herquel, G., Paul, A., 2002. Seismic evidence for stepwise thickening of the crust across the NE Tibetan plateau. Earth Planet. Sci. Lett. 203, 25–33.
Wessel, P., Smith, W.H.F., 1991. Free software helps map and display data. EOS Trans. AGU 72, 441.
Wittlinger, G., Farra, V., Hetenyi, G., Vergne, J., Nabelek, J., 2009. Seismic velocities in Southern Tibet lower crust: a receiver function approach for eclogite detection. Geophys. J. Int. 177, 1037–1049.
Wittlinger, G., Vergne, J., Tapponnier, P., Farra, V., Poupinet, G.J., Su, M., Herquel, H., Paul, G.A., 2004. Teleseismic imaging of subducting lithosphere and Moho offsets beneath western Tibet. Earth Planet. Sci. Lett. 221, 117–130.
Xiao, X., Li, T., 2000. Tectonic Evolution and Uplift Mechanism of the Tibetan Plateau. Guangdong Science Publishing House, Guang Zhou, 313 pp.
Xu, X., Wen, X., Chen, G., Yu, G., 2008. Discovery of the Longriba Fault Zone in Eastern Bayan Har Block and its geotectoinc implication. Sci. China Ser. D 38 (5), 529–542.
Yuan, X., Ni, J., Kind, R., Mechie, J., Sandvol, E., 1997. Lithospheric and upper mantle structure of southern Tibet from a seismological passive source experiment. J. Geophys. Res. 102 (B12), 27491–27500.
Zhang, X., Sun, R., Teng, J., 2007. Study on crustal, lithospheric and asthenospheric thickness beneath the Qinghai-Tibet Plateau and its adjacent areas. Chinese Sci. Bull. 52 (6), 797–804.
Zhang, Z., Klemperer, S.L., 2005. West-east variation in crustal thickness in northern Lhasa block, central Tibet, from deep seismic sounding data. J. Geophys. Res. 110, B09403.
Zhang, Z., Wang, Y., Chen, Y., Houseman, G.A., Tian, X., Wang, E., Teng, J., 2009. Crustal structure across Longmenshan fault belt from passive source seismic profiling. Geophys. Res. Lett. 36, L17310.
Zhao, J., Mooney, W.D., Zhang, X., Li, Z., Jin, Z., Okaya, N., 2006. Crustal structure across the Altyn Tagh Range at the northern margin of the Tibetan plateau and tectonic implications. Earth Planet. Sci. Lett. 241, 804–814.
Zhao, W., Brown, L., Wu, Z., Klemperer, S.L., Shi, D., Mechie, J., Su, H., Tilmann, F., Karplus, M.S., Makovsky, Y., 2008. Seismology across the northeastern edge of the Tibetan plateau. EOS Trans. Am. Geophys. Union 89, 487.
Zhao, W., Mechie, J., Brown, L.D., Guo, J., Haines, S., Hearn, T., Klemperer, S.L., Ma, Y.S.R., Nelson, M.K.D., Ni, J.F., Pananont, P., Rapine, R.A.R., Saul, J., 2001. Crustal structure of central Tibet as derived from project INDEPTH wide-angle seismic data. Geophys. J. Int. 145, 486–498.
Zhao, W., Nelson, K.D., Project INDEPTH Team, 1993. Deep seismic reflection evidence for continental underthrusting beneath southern Tibet. Nature 366, 557–559.
Zhou, B., Peng, J., Zhang, J., 2009. Development and distribution patterns of active fault zones in Qinghai Province. J. Eng. Geol. 17 (5), 612–618.